J_ID: JBC Date: 17-August-20 4/Color Figure(s): F1-7,S2 ART: RA120.014750 Page: 1 Total Pages: 13

JBC ARTICLE

Trapping conformational states of a flavin-dependent *N*-monooxygenase *in crystallo* reveals protein and flavin dynamics

Received for publication, June 23, 2020, and in revised form, July 21, 2020 Published, Papers in Press, July 28, 2020, DOI 10.1074/jbc.RA120.014750

AQ:au Ashley C. Campbell[1], Kyle M. Stiers[1], Julia S. Martin Del Campo[2], Ritcha Mehra-Chaudhary[1], Pablo Sobrado[2,*], and John J. Tanner[1,3,*]

AQ:aff *From the [1]Department of Biochemistry, University of Missouri, Columbia, Missouri, USA, the [2]Department of Biochemistry, Virginia Tech, Blacksburg, Virginia, USA, and the [3]Department of Chemistry, University of Missouri, Columbia, Missouri, USA*

Edited by Joseph M. Jez

The siderophore biosynthetic enzyme A (SidA) ornithine hydroxylase from *Aspergillus fumigatus* is a fungal disease drug target involved in the production of hydroxamate-containing siderophores, which are used by the pathogen to sequester iron. SidA is an *N*-monooxygenase that catalyzes the NADPH-dependent hydroxylation of L-ornithine through a multistep oxidative mechanism, utilizing a C4a-hydroperoxyflavin intermediate. Here we present four new crystal structures of SidA in various redox and ligation states, including the first structure of oxidized AQ:A **SidA without NADP(H) or L-ornithine bound (resting state). The resting state structure reveals a new *out* active site conformation characterized by large rotations of the FAD isoalloxazine around the C1–′C2′ and N10–C1′ bonds, coupled to a 10-Å movement of the Tyr-loop. Additional structures show that either flavin reduction or the binding of NADP(H) is sufficient to drive the** AQ:B **FAD to the *in* conformation. The structures also reveal protein conformational changes associated with the binding of NADP(H) and L-ornithine. Some of these residues were probed using site-directed mutagenesis. Docking was used to explore the active site** AQ:C **of the *out* conformation. These calculations identified two potential ligand-binding sites. Altogether, our results provide new information about conformational dynamics in flavin-dependent monooxygenases. Understanding the different active site conformations that appear during the catalytic cycle may** AQ:D **allow fine-tuning of inhibitor discovery efforts.**

The siderophore biosynthetic enzyme A (SidA) is essential for virulence in *Aspergillus fumigatus* (1, 2), a fungus that infects the lungs and can cause fatal mycoses in humans and other animals. There are around 200,000 new cases of invasive aspergillosis in humans each year, with around half of those resulting in deaths, even when treated with anti-fungal drugs (3). Aspergillosis is particularly harmful in immunocompromised populations (4, 5) and is also a common infection in animals (6, 7). Thus, new anti-fungal drugs are needed in both AQ:E human and veterinary medicine. Knockout of the *SidA* gene in *A. fumigatus* renders the fungus unable to cause disease in mouse models, suggesting that SidA is a good target for therapeutic intervention (1). Because humans and animals lack the *SidA* gene, the inhibition of an equivalent host enzyme is not a restricting factor during treatment or prophylactic use.

SidA is essential for *A. fumigatus* virulence because it is required for siderophore-dependent iron acquisition (8). Iron is an essential nutrient for growth and proliferation of organisms. Iron in the host organism is sequestered by iron-binding proteins, making it a restricted nutrient for *A. fumigatus* and other invasive organisms to acquire (9, 10). Fungi and other infectious organisms have specific metabolic pathways to produce iron-chelating molecules called siderophores (9). Siderophores are peptide-based scaffolds containing iron-chelating groups such as carboxylates, catecholates, and hydroxamates (11), and are used by microorganisms to extract iron from low-iron environments (9, 12). SidA catalyzes the hydroxylation of L-ornithine (L-Orn) to N^5-hydroxyornithine (Scheme 1) (12, 13), S1 which is the first step in the biosynthesis of hydroxamate-containing siderophores (Fig. S1). This is a key step, because the ZSI hydroxyl group added in the SidA reaction is part of the iron-chelating hydroxamate group of the mature siderophore (Fig. ZSI S1). Without the SidA step, the siderophore lacks three of the six oxygen ligands to iron, which would significantly reduce the affinity. The essential role of SidA in siderophore biosynthesis makes it an attractive drug target to impair iron uptake by pathogens (8).

SidA is an *N*-hydroxylating flavin-dependent monooxygenase (NMO) and belongs to a family of enzymes that hydroxylate soft nucleophiles such as the primary amines of lysine and ornithine (14). SidA is a class B flavin monooxygenase, which is characterized by both a high selectivity for its substrate and by $NADP^+$ remaining bound throughout most of the catalytic cycle (Scheme 2) (as opposed to the class A family which are S2 more promiscuous and release $NADP^+$ upon reduction of the flavin) (15–17). SidA contains a tightly bound FAD, which is oxidized in the ligand-free resting state. The catalytic cycle is initiated by the binding of NADPH, resulting in the reduction of the FAD (Scheme 2) (2, 14). The FAD_{red}-$NADP^+$ complex AQ:F reacts with molecular oxygen to form a C4a-hydroperoxyflavin (FAD_{OOH}), with $NADP^+$ remaining bound to the enzyme to stabilize the FAD_{OOH} and thereby preventing H_2O_2 release (*i.e.* uncoupling) (16). L-Orn is then hydroxylated by FAD_{OOH}, and finally N^5-hydroxyornithine and $NADP^+$ are released to complete the cycle (18).

ZSI This article contains supporting information.

* For correspondence: John J. Tanner, tannerjj@missouri.edu; Pablo Sobrado, psobrado@vt.edu.

Trapping conformational states of SidA in crystallo

Several crystal structures of SidA and the related ornithine hydroxylases, PvdA and KtzI, have been determined in various redox and ligation states (Table S1) (19–22). PvdA and KtzI are 37.3% and 33.7% identical in sequence to SidA, respectively, and the three enzymes share a conserved fold and tetrameric structure. The protein fold is composed of three domains: an ornithine binding domain and two Rossmann fold domains, one of which binds FAD and the other NADP(H). The domains are arranged to bring together the *re*-face of isoalloxazine of the FAD, the nicotinamide of NADP(H), and the N5 atom of ornithine for catalysis. These structures have provided information about residues that contribute to substrate and cofactor recognition and insight into the catalytic mechanism.

Motion of the flavin is an important aspect of some flavoenzymes. For example, it has been well established in *p*-hydroxybenzoate hydroxylase, and other related enzymes, that substrate binding induces flavin motion to an exposed position, where it can react with NADPH (16, 23). Flavin reduction then induces motion back to the active site, where catalysis can occur. Also, the flavins in some flavin switch proteins exhibit large redox-linked conformational changes (24). Evidence for flavin dynamics is also emerging for ornithine hydroxylases (22). The SidA structures all show the FAD in a conserved well-ordered state, which will hereafter be termed the *in* conformation. In this conformation the *si*-face of the isoalloxazine is buried and the *re*-face is primed for catalysis. All previously determined SidA structures show the flavin in this in position, regardless of oxidation state or bound ligands (Table S1). The *in* position of the flavin was also observed in PvdA structures in both the oxidized and reduced states (Table S1) (19–21). In contrast, Setser *et al.* (22) described a novel *out* conformation of the oxidized flavin in KtzI in which the *re*-face is buried and not available for catalysis. They also showed that the flavin redox state controls movement between the *in* and *out* conformations (Table S1). This work suggested that flavin dynamics may be an important aspect of the catalytic mechanism of ornithine hydroxylases.

Here we report a new crystal form of SidA that enabled us to capture a new conformation of the FAD and investigate the dependence of the FAD conformation on redox state and ligand binding. Four crystal structures of SidA in different redox and ligation states are reported at high resolution limits of 1.95–2.34 Å (Table 1 and Table S2). The structures reveal information about the role of dynamics in the SidA catalytic mechanism, which could be exploited to identify potential new binding sites for inhibitors.

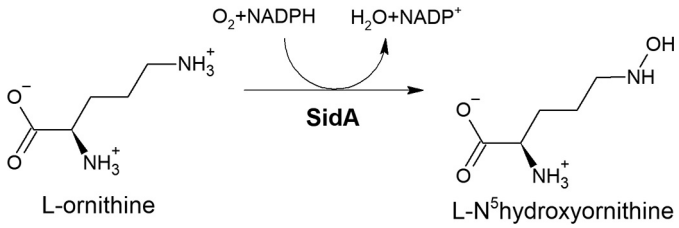

Scheme 1. Reaction catalyzed by SidA.

Results

New crystal form reveals a new flavin conformation

The structure of ligand-free oxidized SidA in a new $P2_1$ crystal form was determined at 2.09Å resolution. This structure represents the resting state of the enzyme, prior to the binding of NADPH. The color of the crystal used for data collection was yellow, consistent with the oxidized state, and no reducing agent was included during crystallization and cryoprotection. The electron density map clearly indicated the conformation of the FAD (Fig. 1*A*). Surprisingly, the isoalloxazine conformation is much different from all previous SidA structures (Fig. 1*B*). In the new conformation, the *re*-face of the isoalloxazine is buried by the protein, whereas the *si*-face stacks against Tyr^{324} (Fig.

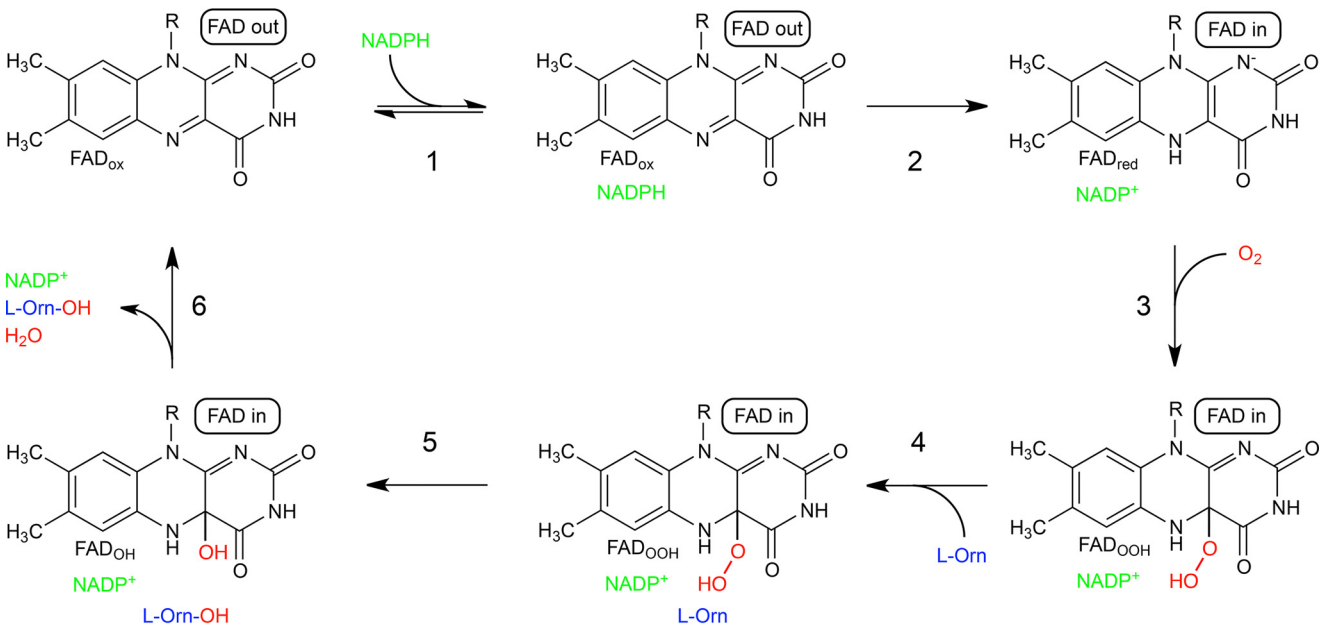

Scheme 2. SidA kinetic mechanism. The conformations of the FAD deduced from this work are indicated in the ovals.

Table 1

AQ:R **Summary of X-ray diffraction and data collection statistics for four crystal structures of SidA in different redox and ligation states**

AQ:S

	FAD_{ox}	FAD_{ox}–$NADP^+$	FAD_{red}–$NADP^+$–L-Orn	FAD_{red}–L-Orn
Resolution (Å)	156.9–2.09 (2.12–2.09)	63.2–1.95 (1.98–1.95)	153.0–2.34 (2.38–2.34)	155.04–2.23 (2.26–2.23)
Mean I/σ^a	6.0 (1.0)	12.1 (1.5)	8.9 (0.8)	7.8 (1.0)
AQ:T $CC_{1/2}{}^a$	0.991 (0.416)	0.997 (0.523)	0.984 (0.8)	0.986 (0.399)
Completeness (%)^a	98.4 (87.4)	99.5 (99.0)	98.5 (71.9)	97.6 (75.2)
$R_{cryst}{}^{a}$	0.1823 (0.2856)	0.1682 (0.2588)	0.1835 (0.2987)	0.2307 (0.3103)
$R_{free}{}^{a,b}$	0.2322 (0.3321)	0.2110 (0.2990)	0.2491 (0.3375)	0.2807 (0.3580)
Clashscore (PR)^c	2.13 (99)	1.78 (100)	2.81 (100)	3.73 (99)
MolProbity score (PR)^c	1.34 (99)	1.09 (100)	1.49 (99)	1.48 (99)
AQ:U Average B (Å^2)				
Protein	37.7	30.2	35.0	57.8
FAD	32.6	23.6	28.6	49.4
L-Orn	N/A	N/A	26.1	41.5
$NADP^+$	N/A	27.6	30.5	N/A
Water	33.9	31.3	30.0	43.0
Protein Data Bank Entry	6X0H	6X0I	6X0J	6X0K

[a] Values for the outer resolution shell of data are given in parenthesis.
[c] 5% test set.
[c] From MolProbity. The percentile ranks (PR) for Clashscore and MolProbity score are given in parentheses.

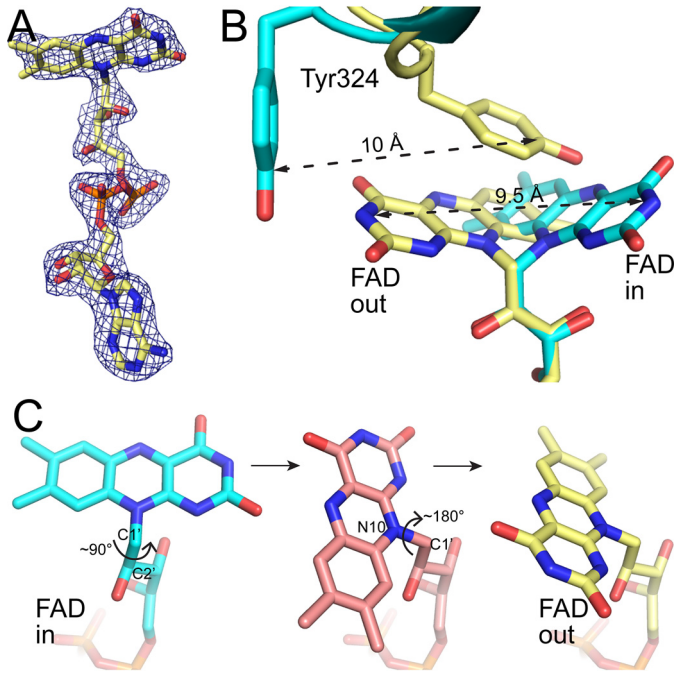

Figure 1. New FAD conformation revealed by the $P2_1$ crystal form. *A*, electron density for the FAD in the oxidized ligand-free $P2_1$ SidA structure. The cage represents a polder omit map (4σ). *B*, superposition of the oxidized ligand-free $P2_1$ SidA structure (*yellow*) and oxidized SidA complexed with L-Orn in space group *I*222 (*cyan*, Protein Data Bank Entry 4B69). *C*, proposed dihedral angle rotations that move the FAD isoalloxazine from the *in* to the *out* conformation.

1*B*). Thus, neither face is available for catalysis. The new structure also shows protein conformational changes that accompany movement of the isoalloxazine. The largest of these involves Tyr^{324}, which moves by 10 Å. The new conformation of the FAD is similar to the *out* conformation described for KtzI (22).

The movement of the FAD between the *in* and *out* conformations appears to involve rotations around two dihedral angles, one of ~90° around the C1′–C2′ bond and another of ~180° around the N10–C1′ bond (Fig. 1*C*). The net result is that the pyrimidine edge moves by 9.5 Å, although the ribityl chain hydroxyl groups are left undisturbed.

Flavin reduction or NADP(H) binding induces movement of the FAD to the in conformation

Crystal soaking and co-crystallization were used to identify conditions that induce movement of the FAD to the *in* conformation observed in all previous SidA structures. Soaking crystals of oxidized, ligand-free SidA with sodium dithionite and L-Orn bleached the yellow color of the crystals, consistent with flavin reduction. In the resulting structure, the isoalloxazine has rotated to the *in* conformation and Tyr^{324} has shifted away from the active site (Fig. 2*B*). Electron density for L-Orn is strong and indicates binding in the expected conformation (Fig. S2*C*). F2 ZSI

Similarly, SidA crystals grown in the presence of $NADP^+$ also show the *in* conformation of the active site (Fig. 2*C*). The *in* conformation was modeled at 100% occupancy in three chains of the asymmetric unit, whereas the density was consistent with dual occupancy of the *in* and *out* conformations in chain C (53% *in*, 47% *out*). Electron density for $NADP^+$ was strong in all four chains, and the ligand was modeled in the conformation observed in other SidA structures (Fig. S2*B*). ZSI

Finally, a crystal of the $SidA_{ox}$-$NADP^+$ complex was soaked AQ:I with NADPH and L-Orn. Soaking bleached the yellow color of the crystals, indicating that NADPH had displaced $NADP^+$ and reduced the flavin. The structure shows that the *in* conformation was maintained in all subunits (Fig. 2*D*).

Altogether, the structures show that either flavin reduction or cofactor binding is sufficient to promote movement of the FAD from *out* to *in*, and that Tyr^{324} moves in concert with the FAD (Fig. 3*A*). We note that Tyr^{324} is part of the Tyr-loop F3 (Asn^{323}-$FTyr^{324}$-Ser^{325}), which is highly conserved among ornithine hydroxylase sequences (see alignment in Fig. S3). The transition from *out* to *in* dramatically changes the structural relationship between Tyr^{324} and the FAD. In the *out* conformation, the two make intimate contact of 3.3 Å (Fig. 3*B*), whereas they are 9.4 Å apart in the *in* conformation (Fig. 3*C*). The stacking of Tyr^{324} against the isoalloxazine in the *out* conformation appears to block the isoalloxazine's path to the *in* conformation, necessitating a concerted 10-Å movement of Tyr^{324} to allow the FAD to rotate around its C1′–C2′ and N10–C1′ bonds into the *in* conformation. Movement of Tyr^{324} is also required for the binding of NADPH. In the *out* conformation of the active site, the stacking ZSI

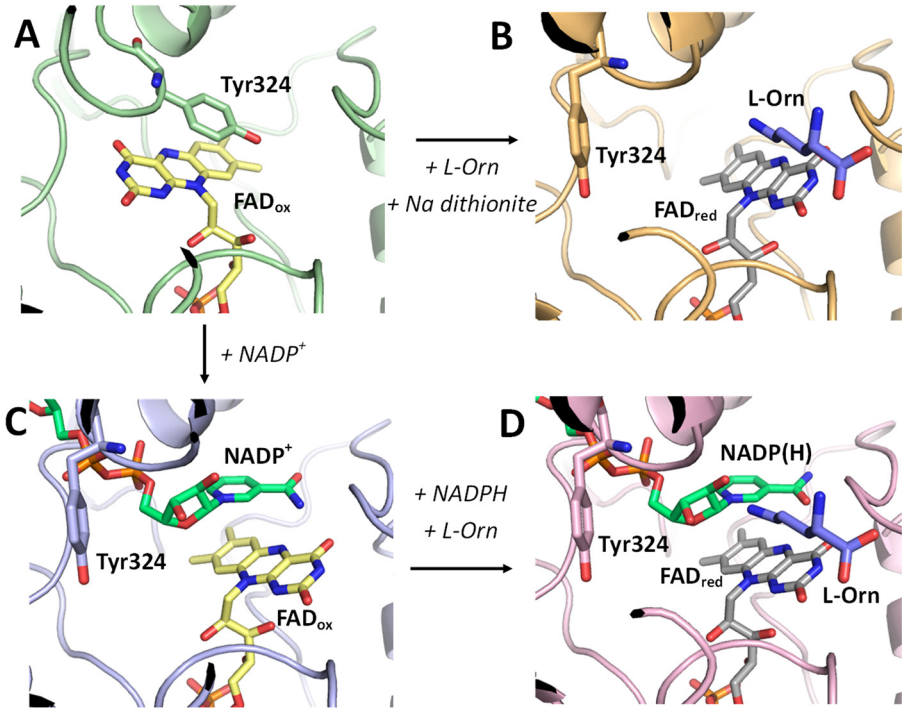

Figure 2. Conformational changes in the active site of SidA. All structures are shown in the same orientation. Oxidized FADs are colored *yellow*; reduced FADs are colored *gray*. *A*, ligand-free oxidized SidA showing the *out* conformation. *B*, dithionite-reduced SidA complexed with L-Orn (*in* conformation). *C*, oxidized SidA co-crystallized with NADP$^+$ (*in* conformation). *D*, NADPH-reduced SidA complexed with NADPH and L-Orn (*in* conformation). Electron density maps ZSI are shown in Fig. S2.

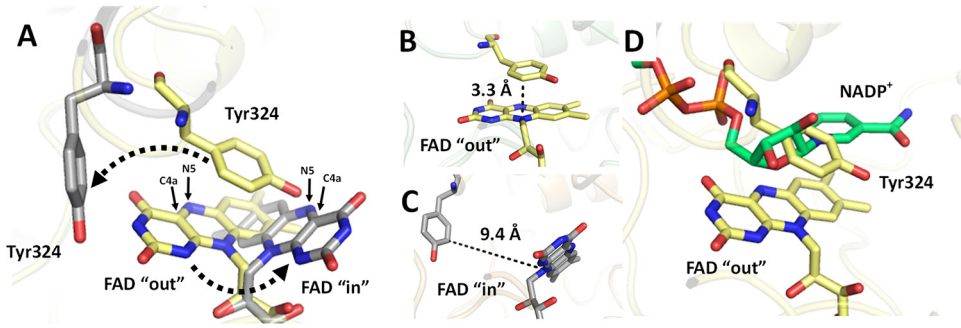

Figure 3. Movements of Tyr^{324} and the FAD are coordinated in SidA. *A*, summary of the major conformational changes between *out* (*yellow*) and *in* (*gray*) states of SidA. The arrows show the direction of movement upon either flavin reduction or NADP$^+$ binding. *B*, distance between Tyr^{324} and the FAD in the resting (*out*) conformation of the active site. *C*, distance between Tyr^{324} and the FAD in the active (*in*) conformation of the active site. *D*, superposition of the resting enzyme conformation (*yellow*) and the NADPH complex (*green*) showing how Tyr^{324} blocks the nicotinamide site.

pose of Tyr^{324} occupies the nicotinamide binding site, necessitating a conformational change to allow cofactor binding (Fig. 3*D*).

Conformational changes associated with ligand binding

By capturing the first structure of SidA in the absence of NADP(H) and L-Orn, we are able to describe the protein conformational changes that accompany cofactor and substrate binding. In addition to Tyr^{324} described above, notable movements involve Asn^{323} and Ser^{325} of the Tyr-loop. Ser^{325} rotates AQ:J 130° around its χ angle upon NADP(H) binding to enable hydrogen bonding with the adenosine phosphate of NADP(H) F4 (Fig. 4, *C* and *D*). The conformational changes for Asn^{323} are more complex than a simple side-chain rotation. The binding of either L-Orn or NADP$^+$ is accompanied by stabilization of Asn^{323}. Electron density for this residue is very weak in three of the subunits of the SidA$_{ox}$ structure, implying high mobility in the absence of ligands. In contrast, Asn^{323} has strong electron density and a well-defined conformation when either NADP$^+$ or L-Orn is present. The stabilization of Asn^{323} likely reflects the hydrogen bonds it forms with the nicotinamide ribose of NADP(H) and the δ-amino group of L-Orn (Fig. 4, *B–D*).

Conformational changes in residues near the Tyr-loop are also observed. Asn^{293} (near Asn^{323}) rotates to hydrogen-bond to the backbone of L-Orn (Fig. 4, *A* to *B* and *C* to *D*). Also, Arg^{279} (near Ser^{325}) rotates to ion-pair with the adenosine phosphate of the cofactor (Fig. 4, *A* to *C*).

Comparison of SidA and KtzI structures

The resting states (oxidized, ligand-free) of SidA$_{ox}$ and KtzI$_{ox}$ (Protein Data Bank Entry 4TM3) share similarities in the

J_ID: JBC Date: 17-August-20 4/Color Figure(s): F1-7,S2 ART: RA120.014750 Page: 5 Total Pages: 13

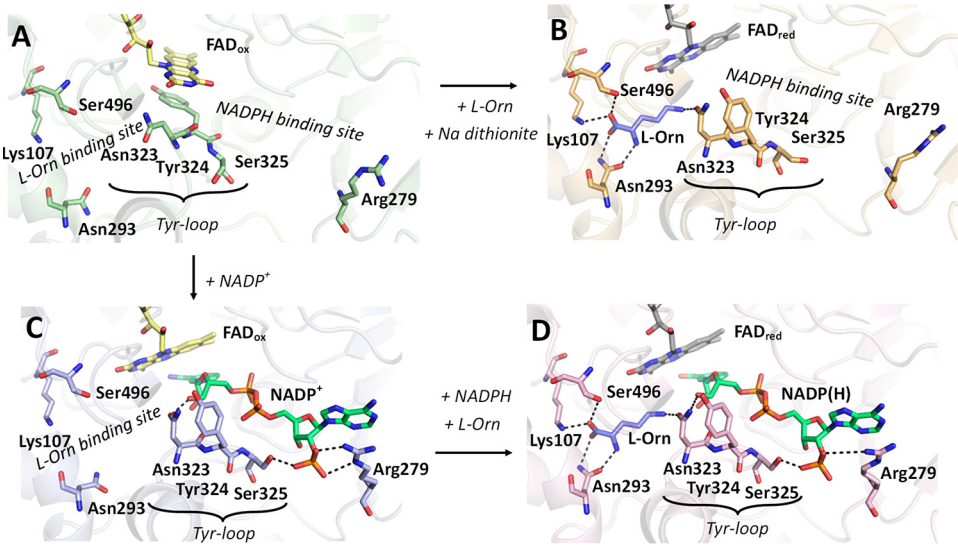

Figure 4. Conformational changes in the active site of SidA are coordinated through the Tyr-loop. *A*, ligand-free SidA (*green*) with oxidized flavin (*yellow*). The FAD is *out*. *B*, L-Orn (*blue*) bound to SidA (*orange*), with the flavin reduced (*gray*) by sodium dithionite. The FAD is *in*. *C*, $NADP^+$ (*green*) bound to SidA (*pale blue*) with oxidized flavin (*yellow*). The FAD is *in*. *D*, L-Orn (*blue*) bound to SidA (*pink*), with the flavin reduced by NADPH (*green*). The FAD is *in*.

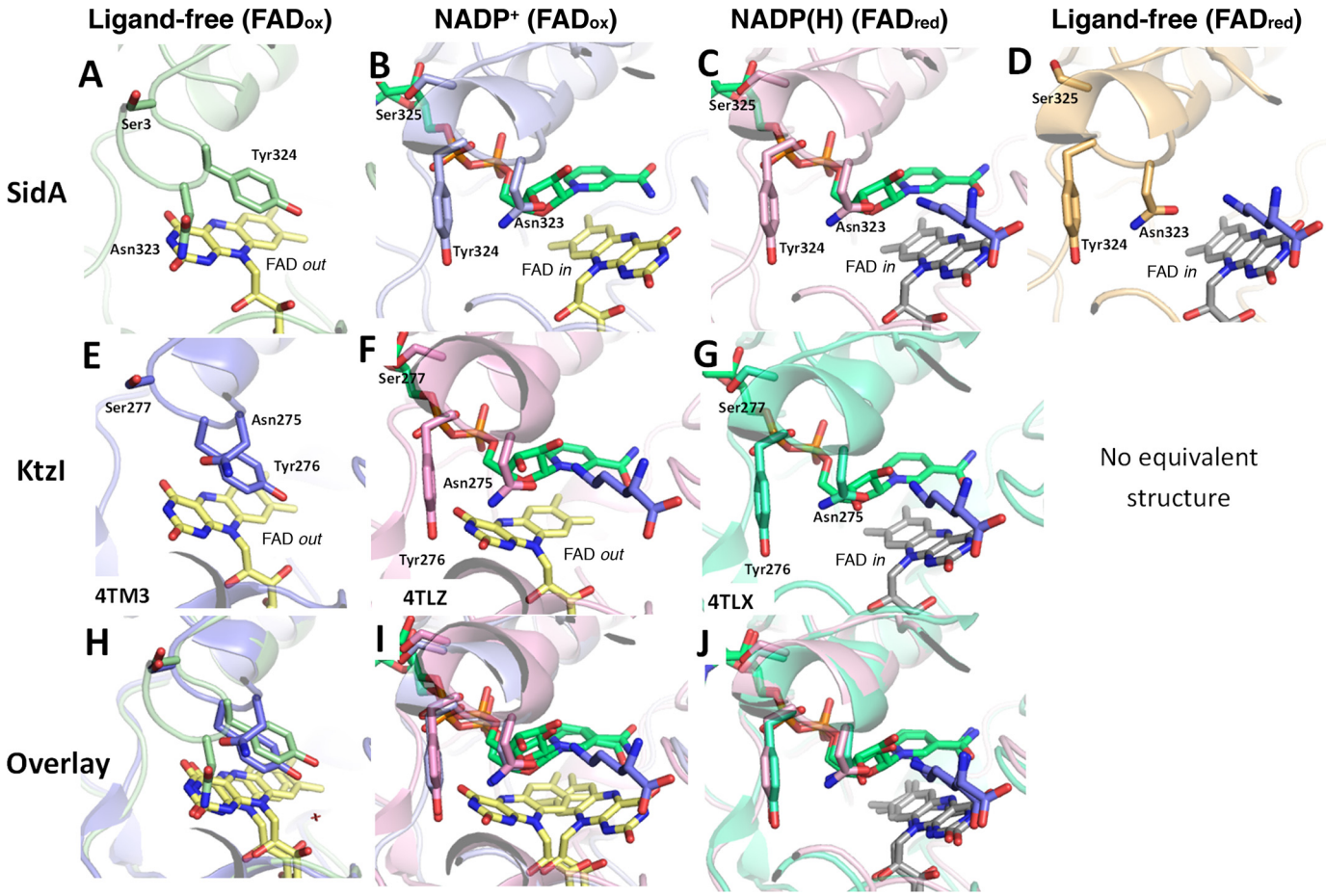

Figure 5. Comparison between equivalent SidA and KtzI structures. The *top row* shows SidA structures representing the following states: *A*, FAD_{ox}–ligand-free, *B*, FAD_{ox}-$NADP^+$, *C*, FADred-NADP(H) and L-Orn, and *D*, FAD_{red} L-Orn. The *middle row* shows KtzI structures representing the following states: *E*, FAD_{ox}–ligand-free (Protein Data Bank Entry 4TM3), *F*, FAD_{ox}-$NADP^+$ (Protein Data Bank Entry 4TLZ), and *G*, FAD_{red}-NADP(H) (Protein Data Bank Entry 4TLX). *H*, overlay of *panel A* and *panel E*. *I*, overlay of *panel B* and *panel F*. *J*, overlay of *panel C* and *panel G*. In all the panels, the Tyr-loop is shown as *sticks*, FAD_{ox} is *yellow*, FAD_{red} is *gray*, and NADP(H) is *green*.

ID: yadavr Time: 17:22 I Path: //mbnas01.cadmus.com/home$/yadavr$/SB-JBCJ200421

Table 2
Kinetic parameters[a] for WT and mutant variants of SidA

	WT	Y324F	CE ratio[b]	H91A	CE ratio[b]	N323A[c]	CE ratio[b]
k_{cat} (s^{-1})	0.59 ± 0.01	0.220 ± 0.005	N/A	0.60 ± 0.2	N/A	1.06 ± 0.06	N/A
$K_{m(l\text{-orn})}$ (mM)	1.0 ± 0.3	9.2 ± 1.5	25	0.40 ± 0.05	0.4	15 ± 1	8
$K_{m(NADPH)}$ (mM)	0.0070 ± 0.0001	0.090 ± 0.001	35	0.017 ± 0.02	2.4	0.010 ± 0.003	0.8
Coupling[d]	~95%	~ 85%	N/A	~28%	N/A	~50%	N/A

[a] The kinetic parameters, k_{cat} and K_m, were obtained from oxygen consumption assays. The table shows the mean and standard deviation of at least two technical replicates.
[b] Catalytic efficiency (k_{cat}/K_m) of WT divided by that of variant.
[c] Data from Robinson, *et al.* (21).
[d] The coupling values were calculated by dividing k_{cat} derived from the oxygen consumption assay by k_{cat} from the iodine oxidation assay.

positioning of the active site residues and the flavin (Fig. 5, *A*, *E*, and *H*). In both structures, the oxidized flavin is in the *out* position with the *re*-face of the FAD buried and the *si*-face stacking with a tyrosine (Tyr^{324} in SidA, Tyr^{276} in KtzI). This shows a conserved active site structure in the resting state of the two ornithine hydroxylases.

The pre-turnover reduced states of SidA and KtzI are also very similar. This state is represented by the structures of $SidA_{red}$-NADPH-Orn and $KtzI_{red}$-NADP-Orn (Protein Data Bank Entry 4TLX). In both structures, the flavin is *in* and the Tyr-loop has been displaced by the NADP(H) cofactor (Fig. 5, *C*, *G*, and *J*).

Curiously, the structures of the oxidized enzymes with $NADP^+$ are different. $SidA_{ox}$-$NADP^+$ has the FAD *in* (Fig. 5*B*), whereas $KtzI_{ox}$-$NADP^+$-Orn has the FAD *out* (Fig. 5*F*). In both structures the Tyr-loop makes an obligatory shift away from the active site to avoid a steric clash with $NADP^+$. These two structures reveal different factors that induce the movement of the isoalloxazine ring. In SidA, we see that the oxidized FAD moves in with $NADP^+$ binding and the nicotinamide of $NADP^+$ stacks with the *re*-face of the isoalloxazine. This suggests that for SidA, cofactor binding can induce the movement of the FAD into the active conformation. In KtzI, the FAD remains *out* even upon cofactor binding. The authors attributed the *out* position of the flavin to its oxidized state and suggested that reduction was required to move the FAD to the *in* conformation (22). Thus, the timing of flavin motion may differ in the two enzymes. As discussed below, our results suggest that the hydride transfer step in SidA could occur with the FAD in an *out* conformation.

Site-directed mutagenesis

We investigated residues that the structures suggest could be important in movement between the *in* and *out* active site conformations. The stacking residue Tyr^{324} was mutated to Ala (Y324A) and Phe (Y324F). Mutation to Ala appears to negatively impact protein folding/solubility, because we were unable to recover any soluble Y324A protein for analysis. Y324F was soluble and exhibited kinetic parameters substantially different from WT. The k_{cat} measured in the oxygen consumption assay was decreased 3-fold, whereas the K_m values for L-Orn and NADPH were increased by ~10-fold (Table 2). Thus, the catalytic efficiencies (k_{cat}/K_m) of Y324F are ~30 times lower than WT. We note that removing the hydroxyl of Tyr^{324} impacts the kinetic parameters much more than removing the side chain of Asn^{323}, a residue that hydrogen-bonds to both NADPH and L-Orn (N323A, Table 2). In particular, the catalytic efficiency of N323A for NADPH is essentially unchanged from WT, whereas that of Y324F is 35 times lower.

We also investigated His^{91} with the mutant variant H91A. His^{91} consistently hydrogen-bonds with the ribityl chain in both the *in* and *out* conformations of the FAD (Fig. S4). The ribityl chain conformation is identical in both conformations, suggesting that residues that interact with the ribityl may be important for limiting the conformational space of the FAD. Mutation of His^{91} to Ala causes no change in k_{cat} and only a modest 2.5-fold increase in the K_m values (Table 2). However, the coupling efficiency of H91A is decreased to 28%, meaning that for every mole of oxygen consumed, only 0.28 mole of HO-N5-Orn is formed. For comparison, the coupling efficiencies of the WT enzyme and Y324F are close to 100% (Table 2).

Probing the out active site of SidA with docking

The *out* conformation of the active site is potentially a new target for inhibitor discovery. We used a fragment-mapping approach (25, 26) to identify potential ligand-binding hot spots. In this approach, sixteen small organic molecules were exhaustively docked to the protein, and the areas where the probe molecules cluster are potential ligand-binding sites.

A control fragment-mapping calculation performed on the *in* structure (Protein Data Bank Entry 6X0I) yielded a large cluster of probes in the NADPH binding site (Fig. 6*A*). In particular, the probes bound preferentially to the nicotinamide dinucleotide site. A smaller cluster of probes corresponded to the δ-amino group of L-Orn (Fig. 6*A*). This control calculation shows that exhaustive docking of small organic molecules has the potential to identify *bona fide* ligand-binding sites in SidA.

An analogous fragment-mapping calculation performed on the *out* conformation also yielded two clusters (Fig. 6*B*). A large, dense cluster of probes was found in a pocket surrounded by Tyr^{324}, Gln^{102}, and Arg^{238}. Note this pocket is separated from the FAD isoalloxazine by Tyr^{324}. The unique conformation of the Tyr-loop makes this pocket exclusive to the *out* state. A more diffuse cluster of probes was found on the surface of the protein near the pyrimidine edge of the FAD (Fig. 6*B*, *cluster 2*). This potential binding surface does not exist in the *in* state, because the pyrimidine edge of the isoalloxazine is inaccessible (Fig. 6*C*). In contrast, the pyrimidine edge pokes out of the NADPH entrance in the *out* state (Fig. 6*D*).

The two potential ligand-binding sites of the *out* conformation were explored further by docking larger compounds. A total of 3035 compounds with molecular weights in the range of 150–300 g/mol were docked to each site. Histograms of the docking energies for the top poses of each compound to the

J_ID: JBC Date: 17-August-20 4/Color Figure(s): F1-7,S2 ART: RA120.014750 Page: 7 Total Pages: 13

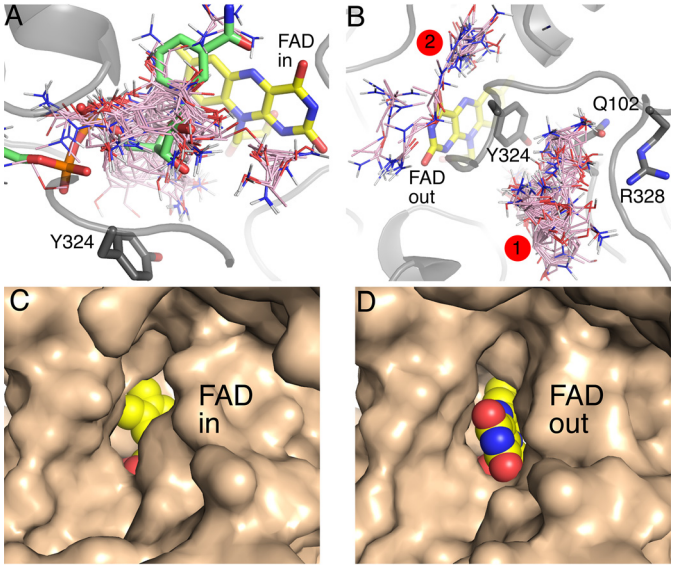

Figure 6. Ligand-binding hot spots from fragment mapping. *A*, results of docking 16 small organic molecules (*pink sticks*) to the *in* conformation of SidA (Protein Data Bank Entry 6X0I). The $NADP^+$ molecule was removed prior to docking but is included here (in *green*) to show that the probes cluster on the nicotinamide dinucleotide binding site. The *smaller cluster* on the right (near the pyrimidine ring of the FAD) corresponds to the location of the δ-amino group of L-Orn. *B*, results of docking 16 small organic molecules (*pink sticks*) to the *out* conformation of SidA (Protein Data Bank Entry 6X0H). *C*, surface representation of the *in* conformation of SidA (Protein Data Bank Entry 6X0I). The FAD is shown in *yellow spheres*. The opening to the active site is the entrance for NADPH. *D*, surface representation of the *out* conformation of SidA (Protein Data Bank Entry 6X0H). The orientation of this view is the same as that in *panel* C.

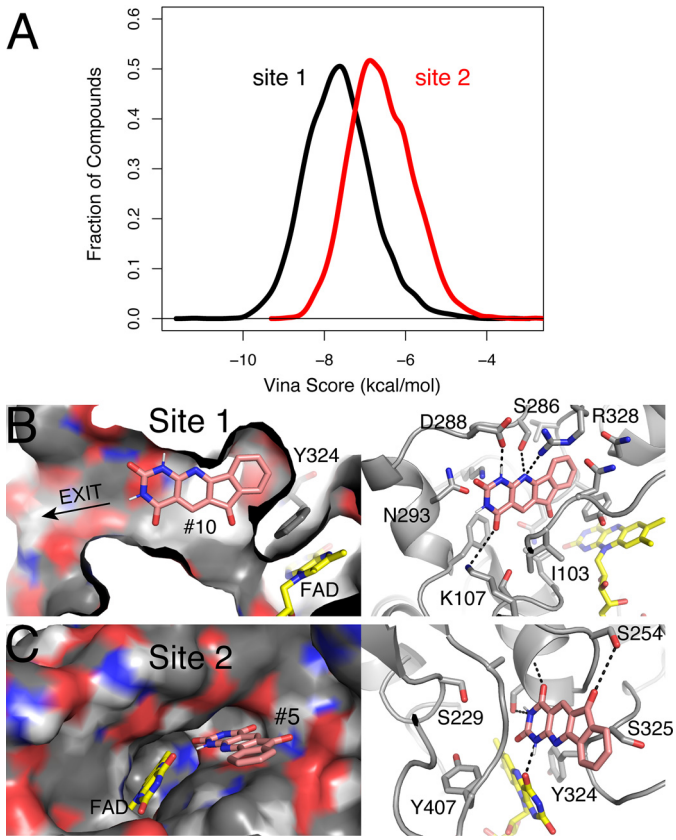

Figure 7. Characterization of potential ligand-binding sites with docking. *A*, histograms of docking scores for the top poses of 3035 compounds docked to site 1 (*black*) or site 2 (*red*) of the *out* conformation of SidA. *B*, The 10th ranked compound for site 1. *C*, the fifth-ranked compound for site 2. Note this is the same compound shown in *panel B*.

two sites are shown in Fig. 7*A*. The peak of the distribution for site 1 is 0.7 kcal/mol more favorable than that of site 2, and over 90% of the compounds have a more favorable score in site 1. The chemical structures of the top 10 ranked compounds for each site are shown in Fig. S5 and Fig. S6 (simplified molecular-input line-entry system strings are listed in Table S3). The physicochemical properties of the top 10 compounds are similar for the two sites (Table S5). In fact, one compound appeared in the top 10 lists of both sites (Fig. 7, *B* and *C*).

Viewing the docked compounds provides insight into the size, shape, and chemical characteristics of the potential binding sites. Site 1 is a true pocket that surrounds the ligand (Fig. 7*B*). The pocket is connected to two tunnels, one leading to the protein surface and another leading to the FAD ribityl chain. Some of the docked compounds have functional groups that access the latter tunnel and interact with the ribityl 3′-hydroxyl. Site 1 has many side chains available for interacting with ligands. The constellation of side chains is diverse, including aromatic, nonpolar, polar, and charged groups (Fig. 7*B*).

Site 2 is rather different. It is a shallow cleft, and the docked ligands have significant solvent-exposed surface area (Fig. 7*C* and Fig. S7). Fewer side chains interact with the docked ligands, and the diversity of side chains in the cleft is lower than that of site 1 (Fig. 7*C*, *right*). Two binding modes were observed among the top 10 compounds. In one mode, the compound accesses the N5 edge of the FAD isoalloxazine (Fig. 7*C*), whereas in the other mode, the compound covers the pyrimidine edge of the FAD (Fig. S7).

Discussion

Here we described a new crystal structure representing the resting state of SidA. The active site is different from all other SidA structures in that the FAD has rotated so that the active face of the isoalloxazine (*re*-face) is buried by the protein and the *si*-face is stacked against the eponymous residue of the conserved Tyr-loop. The resting conformation may offer new opportunities for inhibitor discovery. The docking of probe molecules suggested a preference for a binding site exclusively found in the resting state. Furthermore, this site was lined with residues advantageous for design of inhibitors specific to this conformational state. We also showed by mutagenesis that the stacking residue, Tyr^{324}, is essential for proper catalytic function.

Although atypical for SidA structures, the *out* FAD conformation is very similar to a structure of the resting state of the ornithine hydroxylase KtzI (22). Setser *et al.* (22) referred to the motion of the FAD as "flapping," although as mentioned above, the true molecular motion likely involves two dihedral angle rotations (Fig. 1*C*). The observation of this conformational change in two ornithine hydroxylases with only 34% identity suggests that it may be a conserved dynamic feature of ornithine hydroxylases.

The role of flavin dynamics in the catalytic mechanism remains to be determined. Setser *et al.* (22) have proposed that

ID: yadavr Time: 17:22 I Path: //mbnas01.cadmus.com/home$/yadavr$/SB-JBCJ200421

it helps eject spent $NADP^+$ from the active site following turnover to allow another round of catalysis. Surprisingly, the determinants of flavin dynamics may be different in KtzI and SidA. In KtzI, the oxidation state of the FAD seems to be the key factor, with the reduced FAD always *in* and the oxidized FAD always *out*. In SidA, reduction of the FAD also promotes the *in* state (Fig. 2*B*), but so does co-crystallization of the oxidized enzyme with $NADP^+$ (Fig. 2*C*). Thus, it appears that for SidA, both flavin reduction and cofactor binding may be determinants of the FAD conformation. These results suggest that the role of flavin dynamics in the mechanism is complicated and remains to be unraveled.

Because the *out* conformation is a feature of the resting enzyme, it presumably plays a role in the first step of catalysis, when the FAD is reduced by NADPH (Scheme 2). One possibility is that NADPH reduces the flavin while it is in an *out* conformation. This would require movement of the Tyr-loop, which protects the N5 of the FAD in the *out* state. The reduced flavin would then rotate to the *in* position in unison with $NADP^+$ shifting into the conformation seen in the crystal structures, which is thought to be optimal for stabilization of FAD_{OOH}. Hydride transfer from NADPH to an *out*-like FAD could potentially address the conundrum of the stereochemistry of hydride transfer for class B NMOs. All crystal structures of class B monooxygenases complexed with NADP(H) imply *proS* stereochemistry (*e.g.* Fig. 2, *C* and *D*), yet kinetic studies indicate *proR* stereochemistry (13, 20, 27, 28). Capturing structures of class B NMOs with NADP(H) bound and the FAD in *out*-like conformations represents a new challenge in flavoenzyme structural biology.

Experimental procedures

Protein cloning, expression, and purification

An N-terminally truncated SidA construct was generated by deleting the coding sequence for the first 28 residues of the enzyme (SidAΔ1–28). The truncated gene was cloned into pET15b (Novagen). In the pET15b plasmid, SidAΔ1–28 is expressed with an N-terminal His-tag followed by a thrombin cleavage site. This truncation was chosen because these residues are disordered in previously published structures of SidA (20, 21). We note these N-terminal residues are not present in some other ornithine hydroxylases, including KtzI and PvdA (see alignment in Fig. S3).

SidAΔ1–28 and full-length SidA were expressed in *Escherichia coli* and purified using previously described methods (20). In brief, the protein was expressed in Turbo BL21 (DE3) cells (Genlantis C302020, Fisher Scientific) overnight at 25 °C. The cells were harvested by centrifugation and lysed by sonication in a buffer containing 25 mM HEPES (pH 7.5), 300 mM NaCl, 25 mM imidazole, and 25 mg/ml each of lysozyme, DNase I, and RNase. The protein was purified over a nickel-nitrilotriacetic acid column, washed with 120 mM imidazole, and eluted with 300 mM imidazole. The His-tag was cleaved from full-length SidA using thrombin as described in previous methods (20). The His-tag was not cleaved from SidAΔ1–28. SidAΔ1–28 and full-length SidA for crystallization were dialyzed into a storage buffer containing 25 mM HEPES (pH 7.5) and 100 mM NaCl, flash-frozen in liquid nitrogen, and stored at −80 °C.

Mutagenesis and steady-state kinetics

The WT gene in pET15b was used as a template to make the following amino acid substitutions: Y324A, Y324F, and H91A. Site-directed mutagenesis was performed following the QuikChange system (Agilent Technologies). The genes were sequenced to ensure that the mutations were incorporated. Protein expression and purification was performed as previously described (20). In general, the protein yield was similar to WT SidA, with the exception of Y324A, which was insoluble. The purified proteins were flash-frozen in liquid nitrogen and stored at −80 °C.

The enzyme activity was monitored by measuring either the rate of oxygen consumption or the rate of formation of hydroxylated L-Orn. The rate of oxygen consumption was measured using an Oxygraph system (Hansatech Instruments). Reactions consisted of a 1-ml volume of 100 mM sodium phosphate, pH 7.5, at 25 °C. Hydroxylated ornithine was monitored using a variation of the Csaky iodine oxidation assay (20, 27). The standard assay buffer contained 104 μl of 100 mM sodium phosphate (pH 7.5). NADPH was held constant at 0.5 mM when L-Orn was varied for SidA, H91A (0.1–10 mM), and Y324F (0.1-50 mM). When NADPH was varied (0.01–1.0 mM), L-Orn was present at 10 mM for SidA and H91A and at 60 mM for Y324F. The data were fit to the Michaelis-Menten equation to estimate kinetic parameters.

Crystallization of SidAΔ1–28

A new crystal form was identified by screening SidAΔ1–28 using the Crystal Screen 1 and 2 kits and the Index kit (Hampton Research). Initial screening was done with 8 mg/ml SidAΔ1–28 in the presence of 1 mM $NADP^+$ and 15 mM L-Orn. Small, yellow rod-shaped crystals formed in a condition containing 20% PEG-3350, 0.1 M $MgCl_2$, and 50 mM HEPES (pH 7.5), so this condition was chosen for optimization. Crystal optimization was performed in 24-well plates using the hanging drop vapor diffusion method. Replacing $MgCl_2$ with various salts and optimizing the concentrations of PEG-3350 and HEPES led to the discovery of conditions that yielded larger, more reproducible crystals, which could be grown using either SidAΔ1–28 or full-length SidA, although typically better crystals resulted using SidAΔ1–28. Yellow rod-shaped crystals (0.1–0.2 mm) were reproducible in 17–21% PEG-3350, 0.1 M HEPES (pH 7.5), and 0.1 M calcium acetate. During crystal optimization, crushed seeds from the initial hit were used to streak-seed new drops, using a horse hair. The drop ratio was optimized, resulting in an optimal drop ratio of 2:1 (protein: reservoir). All crystal solutions were prepared with 0.05% sodium azide to prevent fungal growth.

The crystals used in data collection were grown using a reservoir solution of 20% PEG-3350, 0.1 M HEPES (pH 7.5), and 0.1 M calcium acetate, at 20 °C. Microseeding from crushed crystals grown during the optimization stage was important for improving the crystal quality. The hanging drops used to produce crystals for X-ray diffraction consisted of 4 μl SidA (8–10

mg/ml) and 2 μl of the reservoir solution. The volume of the reservoir solution was 500 μl. Upon mixing, the protein solution immediately appeared heavily precipitated, and 24 h later the drops appeared clear. Crystals usually appeared after 2–3 days and grew along the streak-seed line. We note that if microseeding was not used, very large (~1 mm), irregularly shaped crystals that diffracted poorly resulted.

The $SidA_{ox}$ ligand-free structure was determined from a crystal of SidAΔ1–28 grown in the absence of L-Orn or NADP (H). The ligand-free crystals were yellow, consistent with the oxidized state of the FAD. The crystals were prepared for low-temperature data collection by soaking in the cryo-buffer (15% PEG-200, 20% PEG-3350, 0.1 M HEPES, pH 7.5, 0.1 M calcium acetate), followed by flash-cooling in liquid nitrogen.

The $SidA_{ox}$-$NADP^+$ structure was obtained by co-crystallizing full-length SidA with 1 mM $NADP^+$ and 15 mM L-Orn (note that L-ornithine was not built into the active site due to weak density). The $SidA_{ox}$-$NADP^+$ crystals were yellow, confirming the oxidized state of the FAD. The crystals were cryoprotected as described above.

The $SidA_{red}$-NADP(H)-Orn structure was obtained by co-crystallizing SidAΔ1–28 with 1 mM $NADP^+$ and 15 mM L-Orn, and then soaking the crystals in the cryo-buffer supplemented with 100 mM NADPH and 15 mM L-Orn. Upon soaking, the crystals changed from yellow to colorless, demonstrating that the FAD had been reduced by NADPH.

The $SidA_{red}$–L-Orn complex was obtained by soaking crystals of oxidized SidAΔ1–28 in the cryo-buffer supplemented with 100 mM sodium dithionite and 50 mM L-Orn. Upon soaking, the crystals changed from yellow to colorless, demonstrating that the FAD had been reduced by sodium dithionite.

X-ray diffraction, data collection, and refinement

X-ray diffraction data were collected in shutterless mode at beamlines 24-ID-C and 24-ID-E of the Advanced Photon Source (Pilatus 6M and Eiger 16M detectors, respectively), and beamline 4.2.2 of the Advanced Light Source (Taurus-1 CMOS detector). The data were integrated and scaled using XDS (29). Intensities were converted to amplitudes using Aimless (30). The data sets for $SidA_{ox}$, $SidA_{ox}$-$NADP^+$, and $SidA_{red}$-NADP (H)-Orn were processed in space group $P2_1$ and have unit cell dimensions of a = 77–85 Å, b = 153–157 Å, c = 89–91 Å, and β = 109–111°. The asymmetric unit contains a tetramer of SidA. Note the a-axis varies appreciably depending on the ligand and redox state. The space group for $SidA_{red}$ (reduced with sodium dithionite) is also $P2_1$, but apparently soaking in sodium dithionite induced a large change in the unit cell parameters to a = 105.9, b = 155.0, c = 146.85, and β = 91.01°, and the asymmetric unit contains two tetramers of SidA. Data processing statistics are summarized in Table 1 and listed in ZSI detail in Table S2.

The initial phases were determined by molecular replacement. Phaser (31) was used for molecular replacement calculations with a search model derived from chain A of a structure of SidA complexed with $NADP^+$ and L-Orn in the space group $I222$ (Protein Data Bank Entry 4B63) (20). All heteroatoms were removed from the model prior to molecular replacement. PHENIX (32) was used for refinement and Coot (33) was used for model building. Simplified molecular-input line-entry system strings for L-Orn, and $NADP^+$ were used as the input to eLBOW (34) to generate the ligand coordinates and restraint files used during refinement. Structure validation was performed using MolProbity and the wwPDB validation service (35, 36). Refinement statistics are summarized in Table 1 and listed in detail in Table S2. ZSI

Docking calculations

Ligand-binding hot spots were identified using an approach similar to FTMap, in which small organic molecules are docked to the protein (25, 26). Our implementation of the method is as follows. Sixteen probe molecules were docked to the *in* and *out* conformations of SidA using the Autodock Vina 1.1.2 (37): ethanol, isopropanol, isobutanol, acetone, acetaldehyde, dimethyl ether, cyclohexane, ethane, acetonitrile, urea, methylamine, phenol, benzaldehyde, benzene, acetamide, and *N*,*N*-dimethylformamide. To explore all reasonable probe binding pockets, a large search box was defined that encompassed the known binding sites for the FAD, NADP(H), L-Orn, and the connecting solvent-accessible areas. Solvent molecules, NADP (H), and L-Orn were removed from the *in* and *out* structures to prepare them for docking; FAD was retained. The structures were converted to PDBQT format with the AutoDockTools AQ:N program version 1.5.6 (38). Three-dimensional coordinates of probe molecules were generated with Open Babel version 2.3.2 (39). Docking was performed with nine poses for each probe and maximum exhaustiveness of the search box.

The hot spots of the *out* conformation were characterized further by docking larger compounds. The compounds were selected from ChEMBL 27 (40) to have no Lipinski violations and molecular weight in the range of 150–300 g/mol. This filter identified 311,108 compounds. A random selection of ~1% of these compounds (3035) was used for docking. For each site, Autodock Vina was run with 10 poses per compound and maximum exhaustiveness. The physicochemical properties of compounds were calculated with SwissADME (41).

Data availability

The coordinates and structure factors have been deposited in the PDB under accession codes 6X0H, 6X0I, 6X0J, and 6X0K. All other data generated during this study are available within the article and the supporting information. ZSI

Acknowledgments—We thank J. Schuermann and J. Nix for help with remote X-ray diffraction data collection at beamlines 24-ID-C/E and 4.2.2, respectively. We also thank C. Klancher and P. Rodriguez for help with expression and purification of SidA mutant variants. This work is based upon research conducted at the Northeastern Collaborative Access Team beamlines, which are funded by the National Institute of General Medical Sciences from the National Institutes of Health (P30 GM124165). The Pilatus 6M detector on 24-ID-C beam line is funded by a National Institutes of Health-ORIP HEI grant (S10 RR029205). The Eiger 16M detector on 24-ID-E is funded by a NIH-ORIP HEI grant (S10OD021527). This research used resources of the Advanced Photon Source, a AQ:O

United States Department of Energy (DOE) Office of Science User Facility operated for the DOE Office of Science by Argonne AQ:P National Laboratory under contract no. DE-AC02-06CH11357. Beamline 4.2.2 of the Advanced Light Source, a DOE Office of Science User Facility under contract no. DE-AC02-05CH11231, is supported in part by the ALS-ENABLE program funded by the National Institutes of Health, National Institute of General Medical Sciences, grant P30 GM124169-01.

Author contributions—A. C. C., K. M. S., J. S. M. D. C., and R. M.-C. investigation; A. C. C. and J. J. T. writing-original draft; A. C. C., P. S., and J. J. T. writing-review and editing; P. S. and J. J. T. conceptualization; P. S. and J. J. T. funding acquisition; P. S. and J. J. T. project administration; J. J. T. supervision; J. J. T. validation.

Funding and additional information—Research reported in this publication was supported by the National Science Foundation Grants CHE-2003658 (to P. S) and CHE-2003986 (to J. J. T). A. C. C. was funded in part by a Fulbright Science & Innovation Graduate Award.

Conflict of interest—The authors declare that they have no conflicts of interest with the contents of this article.

Abbreviations—The abbreviations used are: L-Orn, L-ornithine; SidA, siderophore biosynthetic enzyme A; NMO, *N*-hydroxylating flavin-dependent monooxygenase.

References

1. Hissen, A. H., Wan, A. N., Warwas, M. L., Pinto, L. J., and Moore, M. M. (2005) The *Aspergillus fumigatus* siderophore biosynthetic gene sidA, encoding L-ornithine N5-oxygenase, is required for virulence. *Infect. Immun.* **73,** 5493–5503 CrossRef Medline
2. Chocklett, S. W., and Sobrado, P. (2010) *Aspergillus fumigatus* SidA is a highly specific ornithine hydroxylase with bound flavin cofactor. *Biochemistry* **49,** 6777–6783 CrossRef Medline
3. Knutsen, A. P., Bush, R. K., Demain, J. G., Denning, D. W., Dixit, A., Fairs, A., Greenberger, P. A., Kariuki, B., Kita, H., Kurup, V. P., Moss, R. B., Niven, R. M., Pashley, C. H., Slavin, R. G., Vijay, H. M., *et al.* (2012) Fungi and allergic lower respiratory tract diseases. *J. Allergy Clin. Immunol.* **129,** 280–291 CrossRef Medline
4. Maschmeyer, G., Haas, A., and Cornely, O. A. (2007) Invasive aspergillosis: epidemiology, diagnosis and management in immunocompromised patients. *Drugs* **67,** 1567–1601 CrossRef Medline
5. Patterson, T. F., Kirkpatrick, W. R., White, M., Hiemenz, J. W., Wingard, J. R., Dupont, B., Rinaldi, M. G., Stevens, D. A., and Graybill, J. R. (2000) Invasive aspergillosis. Disease spectrum, treatment practices, and outcomes. I3 *Aspergillus* study group. *Medicine (Baltimore)* **79,** 250–260
6. Desoubeaux, G., and Cray, C. (2018) Animal models of aspergillosis. *Comp. Med.* **68,** 109–123 Medline
7. Seyedmousavi, S., Guillot, J., Arné, P., de Hoog, G. S., Mouton, J. W., Melchers, W. J., and Verweij, P. E. (2015) *Aspergillus* and aspergilloses in wild and domestic animals: a global health concern with parallels to human disease. *Med. Mycol.* **53,** 765–797 CrossRef Medline
8. Martín Del Campo, J. S., Vogelaar, N., Tolani, K., Kizjakina, K., Harich, K., and Sobrado, P. (2016) Inhibition of the flavin-dependent monooxygenase siderophore A (SidA) blocks siderophore biosynthesis and *Aspergillus fumigatus* growth. *ACS Chem. Biol.* **11,** 3035–3042 CrossRef Medline
9. Wandersman, C., and Delepelaire, P. (2004) Bacterial iron sources: from siderophores to hemophores. *Annu.l Rev. Microbiol.* **58,** 611–647 CrossRef Medline
10. Carver, P. L. (2018) The battle for iron between humans and microbes. *Curr. Med. Chem.* **25,** 85–96 CrossRef Medline
11. Haas, H., Eisendle, M., and Turgeon, B. G. (2008) Siderophores in fungal physiology and virulence. *Ann. Rev. of Phytopathol.* **46,** 149–187 CrossRef Medline
12. Haas, H. (2014) Fungal siderophore metabolism with a focus on *Aspergillus fumigatus*. *Nat. Prod. Rep.* **31,** 1266–1276 CrossRef Medline
13. Romero, E., Fedkenheuer, M., Chocklett, S. W., Qi, J., Oppenheimer, M., and Sobrado, P. (2012) Dual role of NADP(H) in the reaction of a flavin dependent N-hydroxylating monooxygenase. *Biochim. Biophys. Acta* **1824,** 850–857 CrossRef Medline
14. Badieyan, S., Bach, R. D., and Sobrado, P. (2015) Mechanism of N-hydroxylation catalyzed by flavin-dependent monooxygenases. *J. Org. Chem.* **80,** 2139–2147 CrossRef Medline
15. Huijbers, M. M., Montersino, S., Westphal, A. H., Tischler, D., and van Berkel, W. J. (2014) Flavin dependent monooxygenases. *Arch. Biochem. Biophys.* **544,** 2–17 CrossRef Medline
16. Palfey, B. A., and McDonald, C. A. (2010) Control of catalysis in flavin-dependent monooxygenases. *Arch. Biochem. Biophys.* **493,** 26–36 CrossRef Medline
17. van Berkel, W. J., Kamerbeek, N. M., and Fraaije, M. W. (2006) Flavoprotein monooxygenases, a diverse class of oxidative biocatalysts. *J. Biotechnol.* **124,** 670–689 CrossRef Medline
18. Robinson, R. M., Klancher, C. A., Rodriguez, P. J., and Sobrado, P. (2019) Flavin oxidation in flavin-dependent N-monooxygenases. *Protein Sci.* **28,** 90–99 CrossRef Medline
19. Olucha, J., and Lamb, A. L. (2011) Mechanistic and structural studies of the N-hydroxylating flavoprotein monooxygenases. *Bioorg. Chem.* **39,** 171–177 CrossRef Medline
20. Franceschini, S., Fedkenheuer, M., Vogelaar, N. J., Robinson, H. H., Sobrado, P., and Mattevi, A. (2012) Structural insight into the mechanism of oxygen activation and substrate selectivity of flavin-dependent N-hydroxylating monooxygenases. *Biochemistry* **51,** 7043–7045 CrossRef Medline
21. Robinson, R., Qureshi, I. A., Klancher, C. A., Rodriguez, P. J., Tanner, J. J., and Sobrado, P. (2015) Contribution to catalysis of ornithine binding residues in ornithine N5-monooxygenase. *Arch. Biochem. Biophys.* **585,** 25–31 CrossRef Medline
22. Setser, J. W., Heemstra, J. R., Jr, Walsh, C. T., and Drennan, C. L. (2014) Crystallographic evidence of drastic conformational changes in the active site of a flavin-dependent N-hydroxylase. *Biochemistry* **53,** 6063–6077 CrossRef Medline
23. Crozier-Reabe, K., and Moran, G. R. (2012) Form follows function: structural and catalytic variation in the class a flavoprotein monooxygenases. *Int. J. Mol. Sci.* **13,** 15601–15639 CrossRef Medline
24. Becker, D. F., Zhu, W., and Moxley, M. A. (2011) Flavin redox switching of protein functions. *Antioxid. Redox Signal.* **14,** 1079–1091 CrossRef Medline
25. Kozakov, D., Grove, L. E., Hall, D. R., Bohnuud, T., Mottarella, S. E., Luo, L., Xia, B., Beglov, D., and Vajda, S. (2015) The FTMap family of web servers for determining and characterizing ligand-binding hot spots of proteins. *Nat. Protoc.* **10,** 733–755 CrossRef
26. Landon, M. R., Lieberman, R. L., Hoang, Q. Q., Ju, S., Caaveiro, J. M., Orwig, S. D., Kozakov, D., Brenke, R., Chuang, G. Y., Beglov, D., Vajda, S., Petsko, G. A., and Ringe, D. (2009) Detection of ligand binding hot spots on protein surfaces via fragment-based methods: application to DJ-1 and glucocerebrosidase. *J. Comput. Aided Mol. Des.* **23,** 491–500 CrossRef Medline
27. Robinson, R., Franceschini, S., Fedkenheuer, M., Rodriguez, P. J., Ellerbrock, J., Romero, E., Echandi, M. P., Martin Del Campo, J. S., and Sobrado, P. (2014) Arg^{279} is the key regulator of coenzyme selectivity in the flavin-dependent ornithine monooxygenase SidA. *Biochim. Biophys. Acta* **1844,** 778–784 CrossRef Medline
28. Olucha, J., Meneely, K. M., Chilton, A. S., and Lamb, A. L. (2011) Two structures of an N-hydroxylating flavoprotein monooxygenase: ornithine hydroxylase from *Pseudomonas aeruginosa*. *J. Biol. Chem.* **286,** 31789–31798 CrossRef Medline

29. Kabsch, W. (2010) XDS. *Acta Crystallogr. D Biol. Crystallogr*. **66,** 125–132 CrossRef Medline
30. Evans, P. R., and Murshudov, G. N. (2013) How good are my data and what is the resolution? *Acta Crystallogr. D Biol. Crystallogr*. **69,** 1204–1214 CrossRef Medline
31. McCoy, A. J., Grosse-Kunstleve, R. W., Adams, P. D., Winn, M. D., Storoni, L. C., and Read, R. J. (2007) Phaser crystallographic software. *J. Appl. Crystallogr*. **40,** 658–674 CrossRef Medline
32. Afonine, P. V., Grosse-Kunstleve, R. W., Echols, N., Headd, J. J., Moriarty, N. W., Mustyakimov, M., Terwilliger, T. C., Urzhumtsev, A., Zwart, P. H., and Adams, P. D. (2012) Towards automated crystallographic structure refinement with phenix.refine. *Acta Crystallogr. D Biol. Crystallogr*. **68,** 352–367 CrossRef Medline
33. Emsley, P., Lohkamp, B., Scott, W. G., and Cowtan, K. (2010) Features and development of Coot. *Acta Cryst. D Biol. Crystallogr*. **66,** 486–501 CrossRef Medline
34. Moriarty, N. W., Grosse-Kunstleve, R. W., and Adams, P. D. (2009) Electronic ligand builder and optimization workbench (eLBOW): a tool for ligand coordinate and restraint generation. *Acta Crystallogr. D Biol. Crystallogr*. **65,** 1074–1080 CrossRef Medline
35. Chen, V. B., Arendall, W. B., 3rd, Headd, J. J., Keedy, D. A., Immormino, R. M., Kapral, G. J., Murray, L. W., Richardson, J. S., and Richardson, D. C. (2010) MolProbity: all-atom structure validation for macromolecular crystallography. *Acta Crystallogr. D Biol. Crystallogr*. **66,** 12–21 CrossRef Medline
36. Gore, S., Sanz García, E., Hendrickx, P. M. S., Gutmanas, A., Westbrook, J. D., Yang, H., Feng, Z., Baskaran, K., Berrisford, J. M., Hudson, B. P., Ikegawa, Y., Kobayashi, N., Lawson, C. L., Mading, S., Mak, L., *et al.* (2017) Validation of structures in the Protein Data Bank. *Structure* **25,** 1916–1927 CrossRef Medline
37. Trott, O., and Olson, A. J. (2010) AutoDock Vina: improving the speed and accuracy of docking with a new scoring function, efficient optimization, and multithreading. *J. Comput. Chem*. **31,** 455–461 CrossRef Medline
38. Morris, G. M., Huey, R., Lindstrom, W., Sanner, M. F., Belew, R. K., Goodsell, D. S., and Olson, A. J. (2009) AutoDock4 and AutoDockTools4: automated docking with selective receptor flexibility. *J. Comput. Chem*. **30,** 2785–2791 CrossRef Medline
39. O'Boyle, N. M., Banck, M., James, C. A., Morley, C., Vandermeersch, T., and Hutchison, G. R. (2011) Open Babel: an open chemical toolbox. *J. Cheminform*. **3,** 33 CrossRef Medline
40. Davies, M., Nowotka, M., Papadatos, G., Dedman, N., Gaulton, A., Atkinson, F., Bellis, L., and Overington, J. P. (2015) ChEMBL web services: streamlining access to drug discovery data and utilities. *Nucleic Acids Res*. **43,** W612–W620 CrossRef Medline
41. Daina, A., Michielin, O., and Zoete, V. (2017) SwissADME: a free web tool to evaluate pharmacokinetics, drug-likeness and medicinal chemistry friendliness of small molecules. *Sci. Rep*. **7,** 42717 CrossRef Medline

AUTHOR QUERIES

AUTHOR PLEASE ANSWER ALL QUERIES 1

AQau—Please confirm the given-names and surnames are identified properly by the colours as this affects the display and discovery in PubMed and other indexing services.
■=Given-Name, ■= Surname
The colours are for proofing purposes only. The colours will not appear online or in print.

AQaff—Please confirm the following full affiliations or correct here as necessary. This is what will appear in the online HTML version:
[1]Department of Biochemistry, University of Missouri, Columbia, Missouri, USA
[2]Department of Biochemistry, Virginia Tech, Blacksburg, Virginia, USA
[3]Department of Chemistry, University of Missouri, Columbia, Missouri, USA

AQfunding—Au: Can you please confirm or correct the FundRef entries?
1.] Funder Name : National Science Foundation (NSF)
Funder ID : https://dx.doi.org/10.13039/100000001
Grant ID : CHE-2003986
Author(s) : Pablo Sobrado & John J. Tanner
2.] Funder Name : National Science Foundation (NSF)
Funder ID : https://dx.doi.org/10.13039/100000001
Grant ID : CHE-2003658
Author(s) : Pablo Sobrado & John J. Tanner

A—Au: The sentence beginning "Here we present. . ." has been rephrased because it lacked clarity. Please check and confirm edit.

B—Au: Quotes deleted and word italicized throughout due to the frequency used.

C—Au: Quotes deleted and word italicized throughout due to the frequency used.

D—Au: Author: If an ORCID ID is being added for any author when returning corrected proofs, that individual author(s) must also add his/her ORCID ID to his/her eJP submission system profile before it can be added in proofs. Please confirm that this has been done.

E—Au: The Journal makes an effort to follow the gene/protein nomenclature of *Trends in Genetics*. Please check throughout the article to make sure gene/protein designations are styled consistently.

F—Au: Would it be more appropriate to define FADred at first mention or is it OK as-is?

G—Au: In Table 1, it appears that this value may range from 1.95–2.38 Å. Please check and edit if necessary.

H—Au: Is "$P2_1$" an abbreviation? If so, would it be more appropriate to spell it out at first mention?

I—Au: What does SidA_{ox} stand for? Should it be defined at first mention, or is it OK without?

J—Au: The sentence beginning "In addition to Tyr324 described above…" has been rephrased because it lacked clarity. Please check and confirm edit.

K—Au: If meaning of *Km* is "Michaelis-Menten constant, then it is fine as-is. If meaning is something else, please define.

L—Au: "simplified molecular-input line-entry system" as meant by "SMILES"? If not, please define.

M—Au: The sentence beginning "The His-tag was cleaved from…" has been rephrased because it lacked clarity. Please check and confirm edit.

N—Au: What does "PDBQT" stand for? Would it be better to spell it out or is it okay as it is?

O—Au: Sentence beginning "The Eiger 16M detector…" added from NECAT website. Please review and edit if necessary.

P—Au: Please check grant numbers and publication notes for these organizations.

Q—Au: "red" in "FADred" and "ox" in FADox" are not capitalized in text but are capitalized in Fig. 5. Please edit figure or text to match.

R—Au: Table caption has been modified to enhance the ease of understanding. OK?

S—Au: Please check whether the column headings in Table 1 are OK as edited.

T—Au: What does $CC_{1/2}$ stand for here? Would it be more appropriate to spell it out, or is it OK as it is What do the parentheses in this row mean? Please clarify.?

U—Au: Would it be more appropriate to define "*B*" or is it fine as it is?

V—Au: What does "CE" stand for? Would it be more appropriate to spell it out at first mention, or is it OK as written?

W—Au: There are six blank cells in Table 2; if that is intended because there is no data for those cells, please type "N/A" in each empty cell.